AGU PUBLICATIONS

Geophysical Research Letters

RESEARCH LETTER
10.1002/2013GL059182

Key Points:
- The melting behavior of a recently erupted volcanic ash is characterized
- The melting evolution is described in terms of two processes and three main stages
- The high-temperature depositional behavior of volcanic ash is analyzed

Supporting Information:
- Readme
- Movie S1
- Texts S1–S4, Tables S1 and S2, and Figures S1–S13

Correspondence to:
W. Song and D. B. Dingwell,
song.wenjia@min.uni-muenchen.de;
dingwell@lmu.de

Citation:
Song, W., K.-U. Hess, D. E. Damby, F. B. Wadsworth, Y. Lavallée, C. Cimarelli, and D. B. Dingwell (2014), Fusion characteristics of volcanic ash relevant to aviation hazards, *Geophys. Res. Lett.*, *41*, 2326–2333, doi:10.1002/2013GL059182.

Received 31 DEC 2013
Accepted 7 MAR 2014
Accepted article online 12 MAR 2014
Published online 7 APR 2014

Fusion characteristics of volcanic ash relevant to aviation hazards

Wenjia Song[1], Kai-Uwe Hess[1], David E. Damby[1], Fabian B. Wadsworth[1,2], Yan Lavallée[2], Corrado Cimarelli[1], and Donald B. Dingwell[1]

[1]Department of Earth and Environmental Sciences, Ludwig-Maximilians-Universität, Munich, Germany, [2]Earth, Ocean and Ecological Sciences, University of Liverpool, Liverpool, UK

Abstract The fusion dynamics of volcanic ash strongly impacts deposition in hot parts of jet engines. In this study, we investigate the sintering behavior of volcanic ash using natural ash of intermediate composition, erupted in 2012 at Santiaguito Volcano, Guatemala. A material science procedure was followed in which we monitored the geometrical evolution of cylindrical-shaped volcanic ash compact upon heating from 50 to 1400°C in a heating microscope. Combined morphological, mineralogical, and rheological analyses helped define the evolution of volcanic ash during fusion and sintering and constrain their sticking potential as well as their ability to flow at characteristic temperatures. For the ash investigated, 1240°C marks the onset of adhesion and flowability. The much higher fusibility of ash compared to that of typical test sands demonstrates for the need of a more extensive fusion characterization of volcanic ash in order to mitigate the risk posed on jet engine operation.

1. Introduction

Over the past 20 years, the threat from volcanic ash to aviation has been widely recognized and documented [*Casadevall*, 1994; *Miller and Casadevall*, 1999; *Guffanti et al.*, 2009]. In particular, the 2010 eruption of Eyjafjallajökull Volcano in Iceland, which caused major disruptions in air traffic, demonstrated clearly to all societal actors the threat posed by volcanic ash clouds over vast ranges of airspace corridors [*Smith et al.*, 2010; *Sammonds et al.*, 2010; *Matoza et al.*, 2011]. Ash, as is the case for any particulate airborne material, can be ingested into jet engines and can, at higher temperatures, adhere to the internal components of the engine, causing substantial damage [*Pieri et al.*, 2002; *Webley and Mastin*, 2009]. Ultimately, this interaction can result in severe malfunction and in catastrophic engine failure [*Drexler et al.*, 2011]. Moreover, the deposition of volcanic ash inside an engine is exacerbated by the fact that it is the relatively low temperature of the glass transition (approximately ≤ 900°C) rather than the typically substantially higher melting temperatures, at which a viscous liquid will be formed. Thus, the thermal hazard resulting from ash adhesion to engine parts at the comparatively high temperature of the jet engine (1200–1400°C) [*Krotkov et al.*, 1999; *Smith et al.*, 2010] may be far higher for volcanic ash than for other, largely crystalline, airborne particulates. With increasing temperature, volcanic ash transforms (via softening at the glass transition or via melting at the melting point) into liquid silicate fragments whose viscosity relaxation timescale [e.g., *Dingwell and Webb*, 1989], which affect sintering dynamics, decrease with temperature [*Vasseur et al.*, 2013]. Each ash is potentially distinct with respect to its physical state (crystallinity and vesicularity) and its chemical composition (silica content, water content, iron content, etc.). Large variations in both physical state and chemical composition are exhibited between eruptive centers, between eruptive events at a single center, and even during single ongoing eruptive events. In detail, therefore, the fusion and sintering characteristics of volcanic ash are an important variable in the evaluation of the deposition behavior of ingested volcanic ash onto the high-temperature parts of jet engines [*Swanson and Beget*, 1994].

Recent efforts in engineering and material science have focused on the impact of volcanic ash on the operational performance of a jet engine and the integrity of its internal surface materials (e.g., thermal barrier coating) [*Kim et al.*, 1993; *Borom et al.*, 1996; *Krämer et al.*, 2006; *Shinozaki et al.*, 2013]. *Dunn and Wade* [1994] tested the effects of volcanic ash deposition on the operation (turbine temperature, residence time, and pressure) of different gas turbine engines and constrained the minimum turbine inlet temperature required to cause material deposition on hot engine components to 1094°C. *Shinozaki et al.* [2013] investigated the area of a turbine which may be prone to volcanic ash adhesion using as a proxy the temperatures of the gas and turbine surface. They conclude that volcanic ash deposits principally on the nozzle guide vane, causing

local overheating and increase levels of surface roughness, which produces corresponding increases in heat transfer (up to 50%) and surface shear stress coefficient (up to 300%) [*Bons et al.*, 2007].

Simultaneously, efforts to increase the resilience of engines to volcanic ash encounters through the development of more sophisticated protective coatings have been initiated. *Drexler et al.* [2011] developed a novel thermal barrier coating seemingly capable to resist damage from volcanic ash. The coating may, however, not fully prevent volcanic ash from agglutinating to hot parts of a jet engine, as the rheological behavior of ingested volcanic ash (at high temperatures and heating rates), and its control on the dynamics of deposition remains to be tested.

In material science, the sticking potential of material (whether coal ash or here, volcanic ash) at high temperatures has been recognized as a useful parameterization of its propensity for deposition onto hot components of an engine [*Kim et al.*, 1993]. A sticking-potential criterion requires consideration of (1) the onset temperature at which ash is capable of sticking to a hot surface and (2) the time-dependent rheology of the ash as it evolves to a liquid. Decades of work on ash deposition potentials (fouling and slagging) for impurities in fuels in chemical engineering (e.g., coal combustion and gasification) [*Bryers*, 1996; *Vargas et al.*, 2001] as well as studies on melting characteristics of ceramic glazes and different types of industrial glasses [*Pascual et al.*, 2001, 2005; *Dumitrache and Teoreanu*, 2006] have led to the development of characteristic temperatures to assess the sticking ability of fused material. These are (1) the shrinkage temperature (ST), (2) the deformation temperature (DT), (3) the hemisphere temperature (HT), and (4) the flow temperature (FT). This widely employed characterization scheme is yet to be applied in the assessment of volcanic ash hazards.

Here we quantitatively characterize the fusion and sintering dynamics of volcanic ash from 50 to 1400°C and provide a thermomechanical analysis to assess the sticking potential. The parameters obtained are intended to assist in the evaluation of the rheological characteristics of volcanic ash during deposition in jet engines.

2. Experimental Methods

To investigate the fusion characteristics of volcanic ash during heating, we have used the combined approach described in greater detail in the supporting information.

2.1. Volcanic Ash Characterization

For the present study, volcanic ash sampled from the 8 November 2012 eruption of Santiaguito Volcano, Guatemala, was selected due to its currently elevated level of eruptive activity and its hazard potential for aircraft safety [*Bluth and Rose*, 2004; *Ball et al.*, 2013]. The chemical composition, mineralogy, and particle size distribution of the ash sample were obtained using X-ray fluorescence, X-ray diffraction (XRD), and laser diffraction, respectively (Figures S2 and S7, Table S1, and Text S1 in the supporting information).

2.2. Sintering and Thermal Analysis

The sintering behavior of the volcanic ash was determined by monitoring the geometrical evolution of a cylindrically shaped volcanic ash compact (CSVAC) sample in a heating microscope (see Movie S1) [*Boccaccini and Hamann*, 1999]. The experiments were conducted in air at ambient pressure by heating the core samples up to 1400°C at a rate of 10°C min^{-1} (Figures 1a, 1b, and S3). We quantified the change in height, area, and shape factor of the CSVAC sample silhouettes during heating (Figure S4 and Texts S2 and S3), which helped distinguish each of the four characteristic temperatures, ST, DT, HT, and FT. In this manner, it is hoped that a comparison of sintering and thermal analysis behavior under standard experimental conditions will enable us to investigate the relationship between thermal history and the sintering process [*Greco and Maffezzoli*, 2003]. The thermogravimetric and calorimetric behavior of the Santiaguito volcanic ash sample were analyzed using a simultaneous thermal analyzer and differential scanning calorimeter (DSC) from 50 to 1400°C at a rate of 10°C min^{-1}, respectively (Text S1).

2.3. Structural and Mineralogical Analysis

The structural and mineralogical response of the ash sample to heating was studied at 100°C increments (from 100 to 1400°C) by optical microscopy, scanning electron microscopy (SEM), and XRD analysis (Text S1).

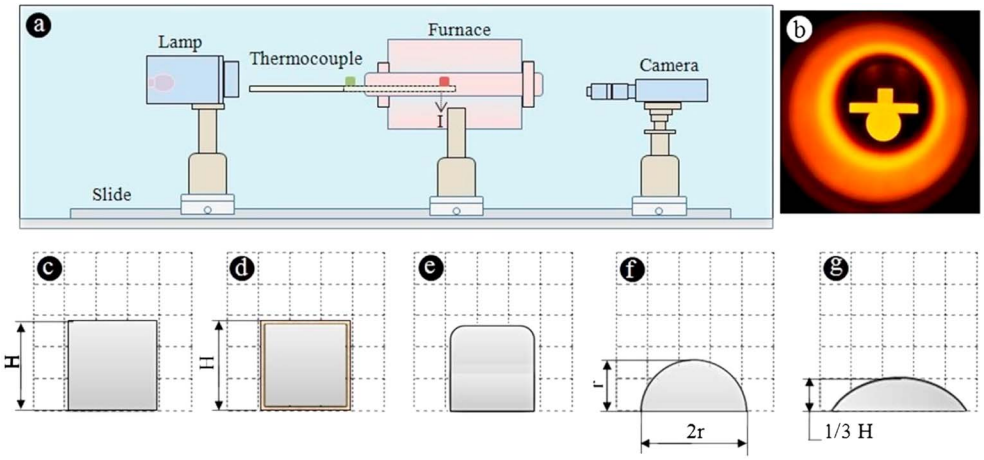

Figure 1. (a) Schematic diagram of the heating microscope used to monitor the sintering process. (b) Photograph of location I in Figure 1. Geometrical definition of the characteristic temperatures in the volcanic ash melting process. (c) Original sample, (d) ST, (e) DT, (f) HT, and (g) FT. ST defines the temperature in which the area of a sample core's silhouette decreases by 5%. DT denotes the temperature initiating the rounding of the corners of a core's silhouette. HT refers to the temperature at which a silhouette approximates a hemisphere. FT marks the point at which the sample is spread over the supporting substrate. (Diagrams in Figures 1c–1g are adapted from CEN/TS 15370-1: 2006 definitions; see Text S3 for details).

2.4. Deposition Behavior Analysis

Each of the four characteristic temperatures was constrained for the volcanic ash by monitoring the silhouette evolution of CSVAC samples (Figures 1c–1g, S5 and S6, and Text S1) while tilting the carriage (alumina substrate) by 70° (Figures S11–S13 and Text S4). In this test, six samples were lined up into the groove of a mold to avoid slipping and simultaneously mounted on the carriage at a given temperature. Upon tilting, one sample was removed to assess the morphology of the initial material. Samples were subsequently removed at 10 min intervals, to allow characterization of the geometrical evolution and thus to constrain the ability of sintered ash to flow.

3. Results

3.1. Sintering Behavior

Figure 2a illustrates the sintering behavior of the Santiaguito volcanic ash sample through quantitative analyses of the geometric changes. The initial change in shape of the ash sample, defined as the point when the area decreased changed by 1.5% of the original test piece area, occurred at 1115°C. We set this temperature as a demarcation point to divide the whole heating profile into two phases, namely, a presintering phase (<1115°C) and a melt-sintering phase (≥1115°C).

During the presintering phase, we monitor two stages of mass loss (Figure 2b). The first event (approximately 4 wt % of the relative weight loss of the sample) occurs near 105 °C and is attributed to adsorbed water dehydration [*Petit and Bandosz*, 2009]. The second mass loss event (75.9 wt % of the relative weight loss of the sample) observed around 470 °C was likely due to dehydroxylation [*Kannan et al.*, 1996]. These mass loss events are constrained by the DSC analysis as endothermic reactions [*Formosa et al.*, 2011] and are accompanied by no changes in the sample mineralogy and microstructures (Figures S7–S10). Sample heating up to this temperature appears to have no effect on subsequent sintering efficiency (Figures 3a–3c).

In the melt-sintering phase, sample melting is evidenced by a broad endothermic peak in the DSC signal (Figure 2b) and results in significant geometric changes (Figure 2a). Such a deformation response is commonly used in material science to constrain the sintering dynamics of fuel ash and glass [*Adell et al.*, 2007; *Bretcanu et al.*, 2009]; here we adopt this scheme. This protocol allows us to further divide the melting-sintering process into three stages defined by geometrical constraints: (1) shrinkage, (2) swelling, and (3) fluxion (Figure 2a) [*Zhang et al.*, 2011].

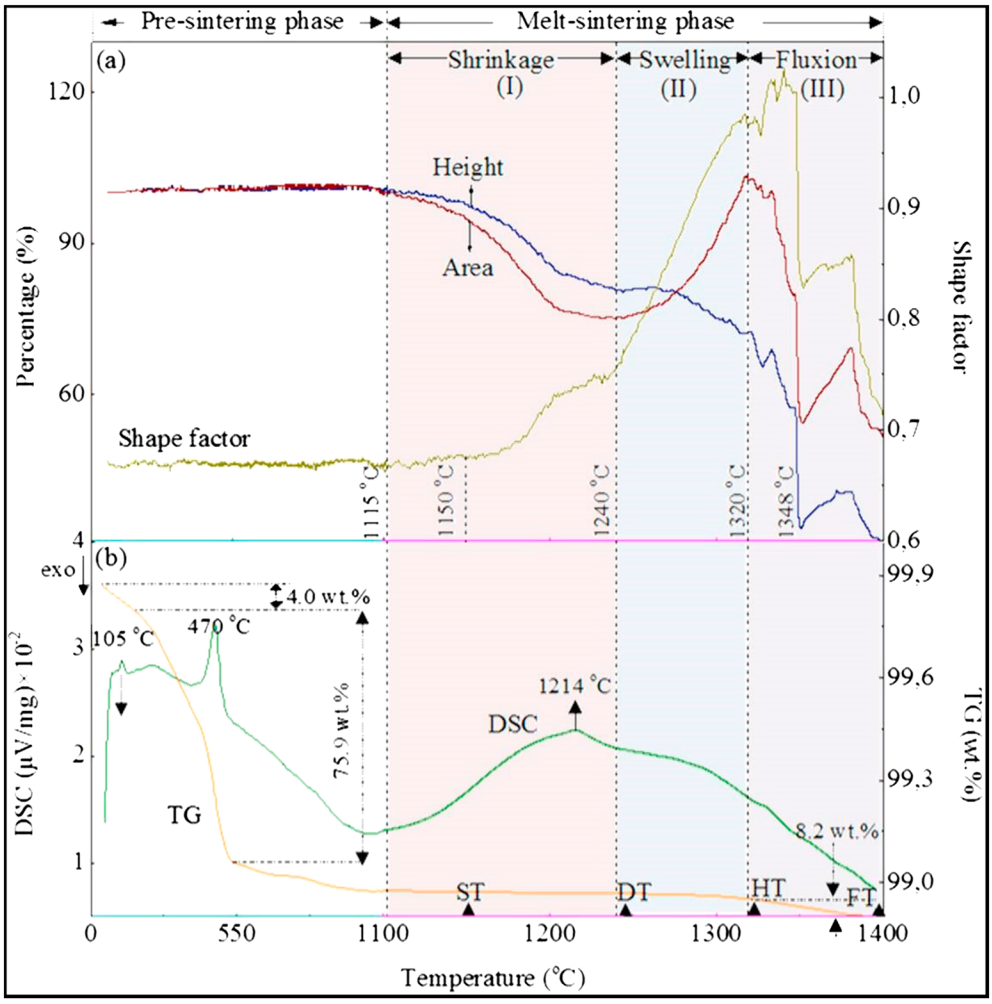

Figure 2. (a) Monitored sintering dynamics of Santiaguito Volcano ash sample. Height, area, and shape factor curves were obtained from microscope image analysis for a CSVAC sample. (b) DSC and derivative TG (DTG) curves for the Santiaguito volcanic ash with a heating rate of 10°C min^{-1}. DSC endothermic and DTG signals in the peaks at ~105°C, at ~470°C, and at ~1320°C are due to the dehydration reaction and dehydroxylation as well as outgassing, respectively, whereas the last DSC endothermic signal in the temperature range 1100–1400°C corresponds to ash melting process.

1. The shrinkage stage (1115–1240°C) corresponds to the temperature range over which a sample silhouette's area and height continuously decrease. Initially, sample shape remains unchanged until at ~1150°C, where the shrinkage temperature, ST, is crossed; the sample silhouette's corners begin to round due to melting until the deformation temperature, DT, is reached (Figures 2a, 3c, and 3d). The morphological response to melting is accompanied by external color changes (Figures 3i and 3j) as well as textural and microstructural developments, following the transition from solid to a liquid; viscous deformation of the ash fragments induces necking at their interfaces, forming an agglutinate frame (Figures 3o versus 3p and 3u versus 3v, respectively). Melting initiates the necking of small, and then larger, particles (Figures 3u and 3v), which likely accounts for the shrinkage of the sample [*Coble*, 1958; *German and Munir*, 1976].
2. The swelling stage (1240–1320°C) is the temperature range over which a sample silhouette's area increases; the expansion is accounted for by extensive widening, yet minor shortening. This response is witness to significant changes in shape of the cylinder into a near sphere, and then hemisphere, defining HT (Figures 3d and 3e). During this stage, the sample is fully molten as can be macroscopically observed from the glassy surface of the end product (Figures 3e, 3k, and 3w). This deformation

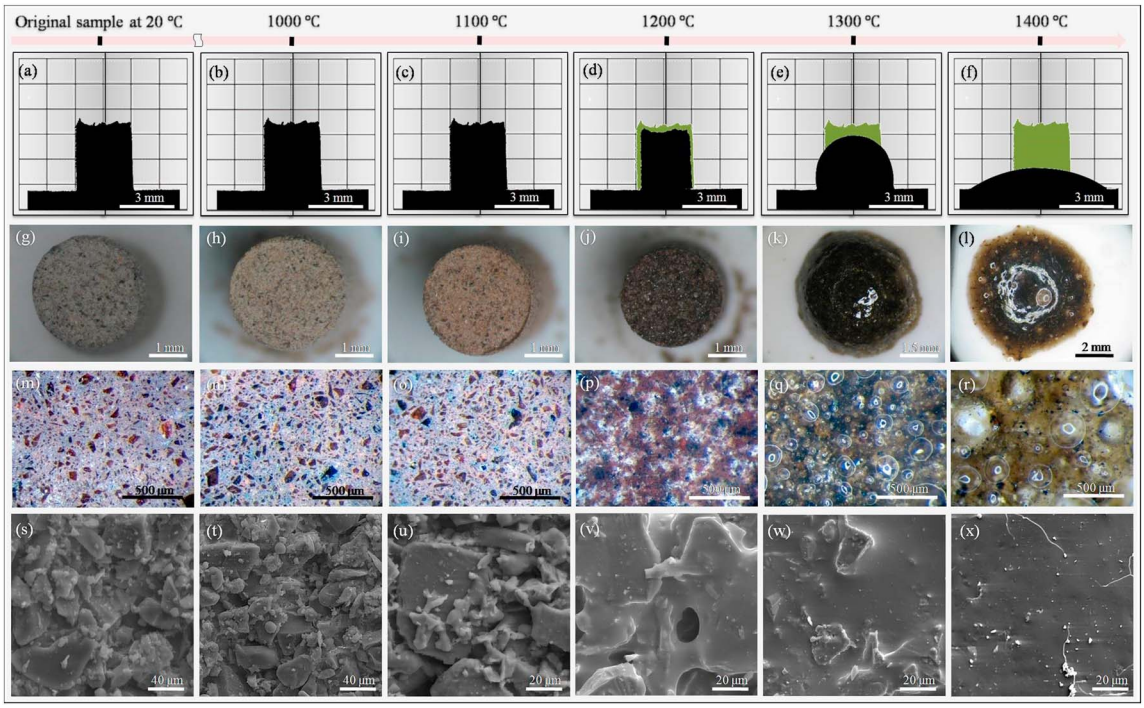

Figure 3. (a–f) Photographs of the sintered CSVAC sample showing the changes in the geometric shape upon heating. (g–l) Photographs showing the progressive fusion and sintering behavior of ash that underline the geometrical changes. (m–r) Photomicrograph and (s–x) SEM image analysis reveal the dominant internal and external microstructures, respectively.

reflects complete necking between particles, which results in the formation and increase in number of isolated bubbles (Figure 3q) [*Vasseur et al.*, 2013]. Upon heating, the bubbles coalesce and expand (both thermally as well as possibly due to the release of volatiles into the bubbles), causing the observed increase in the area of the sample [*Rickard et al.*, 2012].

3. The fluxion stage (1320–1400°C) corresponds to the temperature range over which a sample silhouette's area strongly decreases. This is due to spreading out of the liquid across the alumina substrate due to a reduction in surface tension of the melt with heating. We observe a short period of sample expansion in the fluxion stage (at 1348°C), which is caused by reshaping of the semispherical liquid droplet (with convex contact with the substrate; see Figure 3e) into a spread-out film (with concave contact with the substrate; see Figure 3f), which then in turn flows as the temperature increases further [*Humenik and Kingery*, 1954]. This geometrical transition marks a temperature at which viscosity supersedes surface tension as a key parameter controlling flow and stickiness of the droplet. In the fluxion stage, the height and shape factor mimics the trend of area change (Figure 2a); however, discrepancies in the magnitude of changes are inferred to be the consequence of the outgassing of bubbles from the liquid, as indicated by the TG curves. (Figures 2b, 3 l, 3r and observed in Movie S1)

3.2. Characteristics of Volcanic Ash Deposition

In the foregoing we have characterized the deposition behavior of volcanic ash at ST, DT, HT, and FT through an analysis of the sticking ability and flow distance of the sintered CSVAC samples through time, with the sample on a horizontal and on a tilted substrates (Figures 4a, 4b, and S12). While holding the samples at temperature ST, the samples kept shrinking but did not stick to the substrate, even after 50 min (Figures 4a and 4c). At DT, the samples began to stick to the substrate and flow required 10 min to initiate (Figures 4a and 4d); after 20 min, we measured a constant flow rate (i.e., slope in Figure 4). At HT and FT, the samples flowed readily (Figures 4a, 4e, and 4f); here again, 20 min is required for the flow rate to become steady. We note that the flow rate increases with increasing temperature, due to the lower viscosity of the melt. This morphorheological analysis suggests that the sticking and flow potential of volcanic ash becomes important once temperature reaches the deformation temperature, DT.

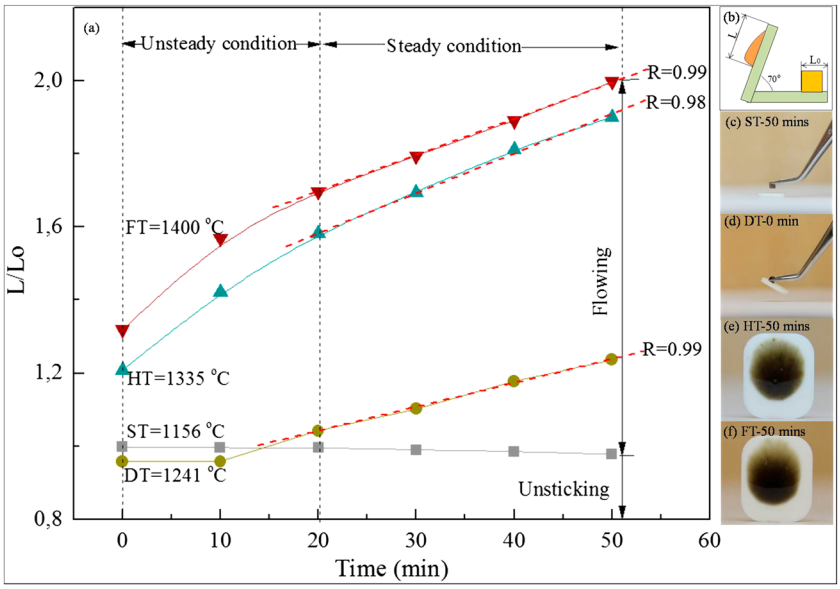

Figure 4. (a) The relative flow of sintered CSVAC samples at each one of the four characteristic temperatures. The plots is complemented by (b) a schematic of the setup and flow measurements before and after tilting the substrate (L_0 = the original distance to the edge of alumina plate, L = the distance after tilting to the edge of alumina plate). The sticking potential is demonstrated as a function of residence time at (c) ST, (d) DT, (e) HT, and (f) FT.

4. Interpretation and Discussion

The results presented in this study illustrate the need for a complete rheological description of volcanic ash across a wide range of temperatures in order to constrain and ultimately mitigate the impacts of volcanic ash on jet engine operation. The fusion and sintering experiments reveal a dynamic deformation and flow behavior, which contrasts with a simple picture of sample rheology. Rheological studies on silicate liquid rheology are typically concerned with the Newtonian behavior of relaxed crystal- and bubble-free melts in equilibrium (i.e., undergoing no changes in phase or chemistry) [e.g., *Dingwell*, 1996], although some recent studies have investigated the effects of crystallization [e.g., *Song et al.*, 2010, 2013]. Traditional rheometers do not allow viscosity determination over as wide a temperature (and viscosity) range as that required to describe fully volcanic ash behavior. A complete description of volcanic ash fusion and sintering dynamics therefore requires consideration of the glass transition, melting, volatile evolution, bubbling, and outgassing —a series of processes which induce a nonlinear rheological response, and which preclude simple non-Arrhenian description based on chemical composition. The experiments presented in this study offer a relationship between characteristic temperatures and the rheology of the material. The tests demonstrate the inability of volcanic ash to stick to a substrate at temperatures below DT—a temperature limit, which ought to be identified when assessing the safety operation of jet engines. Regions of an engine reaching ST should be viewed as being at risk of sticking, without further spreading unless they are subjected to long residency timescales. Above ST, the sticking and flow potential increase rapidly with increasing temperatures (HT and FT) and extended residency may increase damage accumulation.

Sand, which is the particulate most commonly ingested by jet engines, has been used to test turbine operation performance in dust-laden environments. The response of jet engines to the ingestion of foreign particulates strongly depends on their chemical and physical characteristics, yet the literature on this subject has been dominated by sand studies. Due to its liquid origin and high cooling rates, however, volcanic ash usually contains a host glass (i.e., an amorphous phase lacking crystallographic order) which differs both mechanically and rheologically from crystalline sand. A salient observation is that temperatures of sintering and complete melting of Eyjafjallajökull volcanic ash are lower than those of sand by 300°C and 350°C [*Kueppers et al.*, 2014]. Thus, a picture is rapidly emerging in which the impact of volcanic ash deserves separate consideration in order to assess the range of potential hazards on jet engine operation. We propose the protocols defined above as a way forward in this task of utmost importance.

5. Conclusion

This is the first material science study to quantitatively analyze the complex processes of shrinkage, swelling and fluxion of sintering, and melting of volcanic ash. Our analysis of the sticking potential and flow behavior of volcanic ash employing characteristic sintering temperatures highlights the propensity of volcanic ash to impact hot components (of a jet engine) at temperatures exceeding the deformation temperature (defined for volcanic ash, such as from Santiaguito, at 1156°C). This experimental approach remains to be expanded for different heating rates and very importantly, for the breadth of volcanic ash (chemical and mineralogical compositions) state, in order to constrain the potential impact of volcanic ash on jet engine operation.

Acknowledgments

We greatly acknowledge S. Quane and an anonymous reviewer for their constructive reviews. We thank U. Kueppers at LMU and A. Hesse of Hesse Instruments for fruitful discussions. Technical assistance from S. Park, W. Ertl-Ingrisch, and U. Gattermann at LMU as well as C. Wieland and A. Hartung at Technische Universität München is greatly appreciated. W. Song acknowledges Alexander von Humboldt Foundation postdoctoral fellowship. This work was partially funded by the AXA grant "Risk from Volcanic Ash in the Earth System." We acknowledge the European Research Council for the Advanced Grant "EVOKES" (247076) awarded to D.B. Dingwell and the Starter Grant "SLiM" (306488) awarded to Y. Lavallée.

The Editor thanks Steve Quane and an anonymous reviewer for assistance in evaluating this paper.

References

Adell, V., C. R. Cheeseman, M. Ferraris, M. Salvo, F. Smeacetto, and A. R. Boccaccini (2007), Characterising the sintering behaviour of pulverised fuel ash using heating stage microscopy, *Mater. Charact.*, *58*(10), 980–988, doi:10.1016/j.matchar.2006.10.004.

Ball, J. L., E. S. Calder, B. E. Hubbard, and M. L. Bernstein (2013), An assessment of hydrothermal alteration in the Santiaguito lava dome complex, Guatemala: Implications for dome collapse hazards, *Bull. Volcanol.*, *75*, 676, doi:10.1007/s00445-012-0676-z.

Bluth, G. J. S., and W. I. Rose (2004), Observations of eruptive activity at Santiaguito Volcano, Guatemala, *J. Volcanol. Geotherm. Res.*, *136*(3–4), 297–302, doi:10.1016/j.jvolgeores.2004.06.001.

Boccaccini, A. R., and B. Hamann (1999), Review in situ high-temperature optical microscopy, *J. Mater. Sci.*, *34*(22), 5419–5436, doi:10.1023/A:1004706922530.

Bons, J. P., T. H. Fletcher, J. Crosby, J. E. Wammack, and B. I. Bentley (2007), High-pressure turbine deposition in land-based gas turbines from various synfuels, *J. Eng. Gas Turbines Power*, *129*(1), 135–143, doi:10.1115/1.2181181.

Borom, M. P., C. A. Johnson, and L. A. Peluso (1996), Role of environment deposits and operating surface temperature in spallation of air plasma sprayed thermal barrier coatings, *Surf. Coat. Tech.*, *86–87*(1), 116–126, doi:10.1016/S0257-8972(96)02994-5.

Bretcanu, O., X. Chatzistavrou, K. Paraskevopoulos, R. Conradt, I. Thompson, and A. R. Boccaccini (2009), Sintering and crystallisation of 45S5 Bioglass powder, *J. Eur. Ceram. Soc.*, *29*(16), 3299–3306, doi:10.1016/j.jeurceramsoc.2009.06.035.

Bryers, R. W. (1996), Fireside slagging, fouling, and high-temperature corrosion of heat-transfer surface due to impurities in steam-raising fuels, *Prog. Energy Combust. Sci.*, *22*(1), 29–120, doi:10.1016/0360-1285(95)00012-7.

Casadevall, T. J. (1994), The 1989–1990 eruption of Redoubt Volcano, Alaska: Impacts on aircraft operations, *J. Volcanol. Geotherm. Res.*, *62*(1–4), 301–316, doi:10.1016/0377-0273(94)90038-8.

Coble, R. L. (1958), Initial sintering of alumina and hematite, *J. Am. Ceram. Soc.*, *41*(2), 55–62, doi:10.1111/j.1151-2916.1958.tb13519.x.

Dingwell, D. B. (1996), Volcanic dilemma: Flow or blow?, *Science*, *273*(5278), 1054–1055, doi:10.1126/science.273.5278.1054.

Dingwell, D. B., and S. L. Webb (1989), Structural relaxation in silicate melts and non-Newtonian melt rheology in geologic processes, *Phys. Chem. Miner.*, *16*(5), 508–516, doi:10.1007/BF00197020.

Drexler, J. M., A. D. Gledhill, K. Shinoda, A. L. Vasiliev, K. M. Reddy, S. Sampath, and N. P. Padture (2011), Jet engine coatings for resisting volcanic ash damage, *Adv. Mater.*, *23*(21), 2419–2424, doi:10.1002/adma.201004783.

Dumitrache, R. L., and I. Teoreanu (2006), Melting behavior of feldspar porcelain glazes, *U. P. B. Sci. Bull.*, *68*(1), 3–16.

Dunn, M. G., and D. P. Wade (1994), Influence of volcanic ash clouds on gas turbine engines, in *Volcanic Ash and Aviation Safety: Proceedings of the First International Symposium on Volcanic Ash and Aviation Safety*, Bulletin. Ser., vol. 2047, edited by T. J. Casadevall, pp. 107–117, USGS, Washington, D. C.

Formosa, J., J. M. Chimenos, A. M. Lacasta, and L. Haurie (2011), Thermal study of low-grade magnesium hydroxide used as fire retardant and in passive fire protection, *Thermochim. Acta*, *515*(1–2), 43–50, doi:10.1016/j.tca.2010.12.018.

German, R. M., and Z. A. Munir (1976), Surface area reduction during isothermal sintering, *J. Am. Ceram. Soc.*, *59*(9–10), 379–383, doi:10.1111/j.1151-2916.1976.tb09500.x.

Greco, A., and A. Maffezzoli (2003), Polymer melting and polymer powder sintering by thermal analysis, *J. Therm. Anal. Calorim.*, *72*(3), 1167–1174, doi:10.1023/A:1025096432699.

Guffanti, M., G. C. Mayberry, T. J. Casadevall, and R. Wunderman (2009), Volcanic hazards to airports, *Nat. Hazards*, *51*(2), 287–302, doi:10.1007/s11069-008-9254-2.

Humenik, M., and W. D. Kingery (1954), Metal-ceramic interactions: III, Surface tension and wettability of metal-ceramic systems, *J. Am. Ceram. Soc.*, *37*(1), 18–23, doi:10.1111/j.1151-2916.1954.tb13972.x.

Kannan, S., A. Narayanan, and C. S. Swamy (1996), Effect of composition on the physicochemical properties of nickel aluminum hydrotalcites, *J. Mater. Sci.*, *31*(9), 2353–2360, doi:10.1007/BF01152946.

Kim, J., D. P. Wade, E. L. Tremba, M. G. Dunn, and A. J. Baran (1993), Deposition of volcanic materials in the hot sections of two gas turbine engines, *J. Eng. Gas Turbines Power*, *115*(3), 641–651, doi:10.1115/1.2906754.

Krämer, S., J. Yang, C. G. Levi, and C. A. Johnson (2006), Thermochemical interaction of thermal barrier coatings with molten CaO–MgO–Al_2O_3–SiO_2 (CMAS) deposits, *J. Am. Ceram. Soc.*, *89*(10), 3167–3175, doi:10.1111/j.1551-2916.2006.01209.x.

Krotkov, N. A., O. Torres, C. Seftor, A. J. Krueger, A. Kostinski, W. I. Rose, G. J. S. Bluth, D. Schneider, and S. J. Schaefer (1999), Comparison of TOMS and AVHRR volcanic ash retrievals from the August 1992 eruption of Mt. Spurr, *Geophys. Res. Lett.*, *26*(4), 455–458, doi:10.1029/1998GL900278.

Kueppers, U., C. Cimarelli, K.-U. Hess, J. Taddeucci, F. B. Wadsworth, and D. B. Dingwell (2014), The thermal stability of Eyjafjallajökull ash versus turbine ingestion test sands, *J. Appl. Volcan.*, *3*, 4, doi:10.1186/2191-5040-3-4.

Matoza, R. S., et al. (2011), Long-range acoustic observations of the Eyjafjallajökull eruption, Iceland, April–May 2010, *Geophys. Res. Lett.*, *38*, L06308, doi:10.1029/2011GL047019.

Miller, T. P., and T. J. Casadevall (1999), Volcanic ash hazards to aviation, in *Encyclopedia of Volcanoes*, edited by H. Sigurdsson et al., pp. 915–930, Academic, San Diego, Calif.

Pascual, M. J., L. Pascual, and A. Durán (2001), Determination of the viscosity-temperature curve for glasses on the basis of fixed viscosity points determined by hot stage microscopy, *Eur. J. Glass Sci. Technol.*, *42*(1), 61–66.

Pascual, M. J., A. Durán, and M. O. Prado (2005), A new method for determining fixed viscosity points of glasses, *Eur. J. Glass Sci. Technol.*, *46*(5), 512–520.

Petit, C., and T. J. Bandosz (2009), Graphite oxide/polyoxometalate nanocomposites as adsorbents of ammonia, *J. Phys. Chem. C*, *113*(9), 3800–3809, doi:10.1021/jp8097044.

Pieri, D., C. Ma, J. J. Simpson, G. Hufford, T. Grindle, and C. Grove (2002), Analyses of in-situ airborne volcanic ash from the February 2000 eruption of Hekla Volcano, Iceland, *Geophys. Res. Lett.*, *29*(16), 19-1–19-4, doi:10.1029/2001GL013688.

Rickard, W., J. Temuujin, and A. van Riessen (2012), Thermal analysis of geopolymer pastes synthesised from five fly ashes of variable composition, *J. Non-Cryst. Solid*, *358*(15), 1830–1839, doi:10.1016/j.jnoncrysol.2012.05.032.

Sammonds, P., B. McGuire, and S. Edwards (2010), Volcanic hazard from Iceland: Analysis and implications of the Eyjafjallajökull eruption, *Tech. Rep.*, UCL Institute for Risk and Disaster Reduction, London, U. K.

Shinozaki, M., K. A. Roberts, B. van de Goor, and T. W. Clyne (2013), Deposition of ingested volcanic ash on surfaces in the turbine of a small jet engine, *Adv. Eng. Mater.*, *15*(10), 986–994, doi:10.1002/adem.201200357.

Smith, R. A., C. Brown, R. Martinez-Botas, P. Reading, S. Tetlow, and P. Watson (2010), Volcanic ash: To fly or not to fly, *Tech. Rep.*, Inst. Mech. Eng., London, U. K.

Song, W., Y. Sun, Y. Wu, Z. Zhu, and S. Koyama (2010), Measurement and simulation of flow properties of coal ash slag in coal gasification, *AIChE J.*, *57*(3), 801–818, doi:10.1002/aic.12293.

Song, W., L. Tang, Z. Zhu, and Y. Ninomiya (2013), Rheological evolution and crystallization response of molten coal ash slag at high temperatures, *AIChE J.*, *59*(8), 2726–2742, doi:10.1002/aic.14052.

Swanson, S. E., and J. Beget (1994), Melting properties of volcanic ash, in *Volcanic Ash and Aviation Safety: Proceedings of the First International Symposium on Volcanic Ash and Aviation Safety*, Bulletin. Ser., vol. 2047, edited by T. J. Casadevall, pp. 87–92, USGS, Washington, D. C.

Vargas, S., F. J. Frandsen, and K. Dam-Johansen (2001), Rheological properties of high-temperature melts of coal ashes and other silicates, *Prog. Energy Combust. Sci.*, *27*(3), 237–429, doi:10.1016/S0360-1285(00)00023-X.

Vasseur, J., F. B. Wadsworth, Y. Lavallée, K.-U. Hess, and D. B. Dingwell (2013), Volcanic sintering: Timescales of viscous densification and strength recovery, *Geophys. Res. Lett.*, *40*, 5658–5664, doi:10.1002/2013GL058105.

Webley, P., and L. Mastin (2009), Improved prediction and tracking of volcanic ash clouds, *J. Volcanol. Geotherm. Res.*, *186*(1–20), 1–9, doi:10.1016/j.jvolgeores.2008.10.022.

Zhang, Z., X. Wu, T. Zhou, Y. Chen, N. Hou, G. Piao, N. Kobayashi, Y. Itaya, and S. Mori (2011), The effect of iron-bearing mineral melting behavior on ash deposition during coal combustion, *Proc. Combust. Inst.*, *33*(2), 2853–2861, doi:10.1016/j.proci.2010.07.061.